Supporting Information

Direct Evidence of Fe(V) and Fe(IV) Intermediates during Reduction of Fe(VI) to Fe(III): Nuclear Forward Scattering of Synchrotron Radiation Approach

Libor Machala,[1*] Vít Procházka,[1] Marcel Miglierini,[1,2] Virender K. Sharma,[3] Zdeněk Marušák,[1] Hans-Christian Wille,[4] Radek Zbořil[1*]

1 Regional Centre of Advanced Technologies and Materials, Departments of Experimental Physics and Physical Chemistry, Faculty of Science, Palacký University, Šlechtitelů 11, 783 71 Olomouc, Czech Republic

2 Institute of Nuclear and Physical Engineering, Slovak University of Technology, Ilkovicova 3, 812 19 Bratislava, Slovakia

3 Department of Environmental and Occupational Health, School of Public Health, Texas A&M University, 1266 TAMU, College Station, Texas 77843, USA

4 DESY, Notkestraße 85, D-22607 Hamburg, Germany

E-mail: libor.machala@upol.cz, radek.zboril@upol.cz

^{57}Fe-enriched solid K_2FeO_4 sample

A two-step process was used to prepare an aqueous solution of $Fe(NO_3)_3 \cdot 9H_2O$ enriched by ^{57}Fe isotope, which served as a precursor for the ferrate(VI) synthesis. The enrichment is labelled as ^{57}Fe in the following text. Firstly, ^{57}Fe ferric chloride was prepared by dissolution of ^{57}Fe hematite in a stoichiometric amount of hydrochloric acid. In the second step, ^{57}Fe ferric chloride was combined with silver nitrate in an aqueous metathesis reaction. The precipitate of silver chloride was filtered out from the solution. The excess liquid was evaporated by a dry nitrogen flow at room temperature due to the low thermal stability of ferric nitrate solution.

A powdered (^{57}Fe) K_2FeO_4 sample was prepared according to the method of Thompson et al.[1] Briefly, oxidation of (^{57}Fe) $Fe(NO_3)_3 \cdot 9H_2O$ by hypochlorite in a 14 M NaOH solution resulted in sodium ferrate(VI) (Na_2FeO_4), which was then precipitated as (^{57}Fe) K_2FeO_4 by adding solid KOH. The prepared crystals were then dried in ethanol and stored in a vacuum desiccator.

The powdered K_2FeO_4 had a grain size in the range of 1-100 μm (Fig. S1a). The purity of the sample was tested using ^{57}Fe NFS at room temperature (Fig. S1b). The sample contained 98 % Fe(VI) and the remaining 2 % was Fe(III), corresponding to ferric hydroxide. The series of NFS time spectra of a powdered K_2FeO_4 were collected at the Dynamics Beam line at PETRAIII,[2] DESY, Hamburg, Germany. The K_2FeO_4 was introduced into a glass capillary with a diameter of 1.2 mm before it was placed into the furnace (Linkam THMS600).

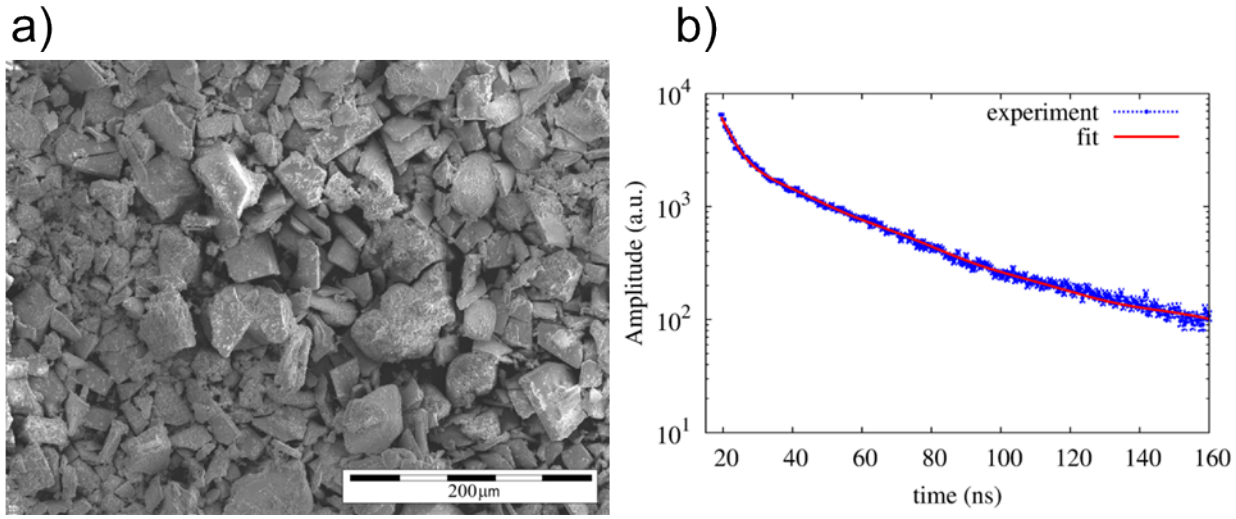

Fig. S1. a) Scanning electron microscope (SEM) image of (^{57}Fe) K_2FeO_4 powder; b) Nuclear forward scattering time spectrum of (^{57}Fe) K_2FeO_4 sample fitted by a major singlet component (98 % Fe) corresponding to K_2FeO_4 and a minor component (2 % Fe) related to ferric hydroxide.

Synchrotron experiments

Nuclear forward scattering (NFS) belongs to the family of hyperfine methods based on the nuclear level excitation and Mössbauer effect.[3] All resonant nuclei in the sample are coherently excited by a beam of synchrotron radiation and followed by a coherent deexcitation connected with gamma-quanta emission. This results in a time spectrum, where information about the hyperfine structure of the sample is encoded. Due to the high brilliancy of synchrotron radiation, which induces the excitation of the nuclei, together with the usage of samples enriched by ^{57}Fe isotope, the time needed for the detection of one relevant time spectrum[4] of a sufficient quality is reduced to approximately one minute. This makes the NFS an excellent tool with good time resolution of the chemical state for a thorough *in-situ* study of the mechanism and kinetics of the thermal decomposition process of potassium ferrate(VI). Monochromated linearly polarized radiation with energy of 14.4 keV and energy resolution of 1 meV was applied to the sample in a spot of 1×2 mm. The photon flux was $7 * 10^{13}$ ph s^{-1}.

Evaluation of NFS spectra

Each NFS time spectrum was accumulated and recorded within the time interval of one minute, with repeated NFS time spectra collected (a few seconds between two successive records were consumed follow for memory storing and software/hardware processing). Thus, in total 173 time spectra were acquired during a time period of 210 min including the heating from room temperature to 235 °C and isothermal heating at 235 °C. The acquired time spectra were analyzed by the CONUSS software. [5] The detection limit of the NFS technique is approximately one percent. Since contents of the intermediate species were only a few percent above this limit, special attention was paid to the data analysis procedure. A number of theoretical models for reconstruction of the time spectra were proposed and tested in order to identify the most relevant one. A model with initial values of hyperfine parameters already known for K_2FeO_4 and $KFeO_2$ was used to calculate the theoretical time spectrum, which was compared with the experimental one. Next, the hyperfine parameters were varied in order to obtain the best fit of the theoretical curve to the experimental data. The chi-square test was used as a criterion for fitting the curve. In some general cases, a reduced chi-square is reliable for comparing the applicability of different models. However, this was not relevant for our study because all points obtained in the time spectra were supposed to be independent and also experimental points in one time spectrum were high.

Initially, the simple two-component model was applied to analyze the data. The chi-square parameter exceeded certain values depending on the annealing time. This indicated the presence of other phases in the sample. This analysis was followed by testing of additional fitted models having three, four, and five different spectral components. The incorporation of additional components into the fitted

models significantly improved statistical quality of the fits. However, the improvements were hardly seen visually since the data were presented in a log scale and thus enhanced observations of lower intensities. This was in contrast to the fitting procedure which was more sensitive to higher intensities than lower intensities. Therefore, the quantum beats that exhibit proper oscillations in the log plots were controlled. Simultaneously, we monitored the decrease of the chi-square parameter, which quantitatively reflected the integral improvement of the fit. Fig. S2 compares the fits using models with two and five components.

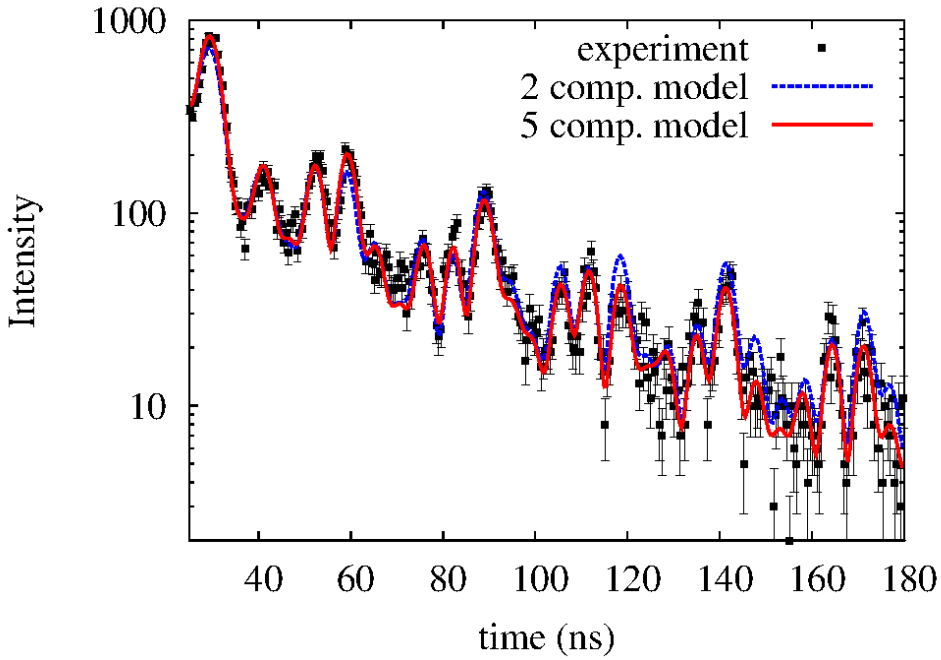

Fig. S2. Comparison of two-component and five-component fitted models for the experiment at the 50th minute of annealing.

Fig. S3 presents the evolution of the chi-square parameter for all the fitted models during the annealing process. The individual components are marked as A, B, C, D, and E. During the fitting of four components, we observed that there were two ranges: a higher amount of the fourth component, separated by a minimum where the amount of the component decreased below 1 %. The first maximum corresponded to an isomer shift of –0.55 mm/s; the second maximum exhibited an isomer shift of –0.3 mm/s. Because there was no significant overlap between these two entities, two ranges were interpreted as two separate components with fixed values of isomer shift, which were precisely determined from the corresponding NFS time spectra. Consequently, we present the two four-component models, where component (B) or (D) is missing. These models are labeled as \$4B and \$4D while other models are labeled by symbols \$2, \$3 and \$5 (Fig. S3).

Fig. S3 clearly shows that the five-component fitted model fit the experimental data better than the other tested models over the entire period of the annealing process. However, values of chi-square were strongly affected by the intensity of the synchrotron radiation, which oscillated due to monochromator instabilities. Higher intensity of the incident radiation caused higher intensity of the scattered radiation and consequently higher relative accuracy of the measurement. Therefore, the chi-square increased when the intensity of the beam increased. In order to avoid this effect in comparison of two models, it was better to calculate the ratios of the chi-squares corresponding to two given fitted models.

In Fig. S4, the chi-square values corresponding to the two-, three-, and four-component models are compared with the chi-square values obtained using the five-component model within the period between 20th and 100th minute of the experiment. In this time range, the majority of the transformations were observed. Fig. S4 shows that the models with three, four and five components satisfied the experimental data at the beginning of the decomposition. The chi-square for the two- component model \$2 is significantly 30% higher over the entire period of time. Up to minute 40 of the decomposition process, models \$3, \$4B, \$4D, and \$5 were in good agreement with the experimental data and the chi-square values differed less than by 10 %. Beginning minute at 40, the chi-square increased by approximately 20 % for models \$3 and \$4D in relation to the \$5 model. The chi-square for the \$4B model was still just 5 % above the chi-square for the \$5 model. In the period from the 40th to the 60th minute, component (B) ascribed to iron(V) was observed. When the (C) component occurred at ~ 50 min, the chi-square increased slightly. When the amount of component (D) increased after 70 minutes, the chi-square became higher with respect to the \$5 model. In contrast, the chi-square for the \$4D model decreased after 70 minutes. This occurred because component (B) was almost non-existent before the 70th minute, but increased after minute 70. Therefore, the \$4D model was selected over the \$4B model. The chi-square of the 4D\$ model approached the chi-square of the \$5 model after minute 90 because component (B) disappeared and therefore did not affect the fit of the model.

These data clearly demonstrate that the five-component model could be easily replaced by the model containing only four components since the overlap of the ranges with significant amounts of components (B) and (D) were rather small. It would be the most appropriate for the interpretation to use the five-components model which was physically equivalent with that containing four components. In order to exclude any correlations between the fitting parameters, a set of fittings was also performed where different parameters were fixed and released. All the results were compared and the best were selected, based on a satisfactory agreement in the quality and quantity of the parameter. Overall, the in-depth precise evaluation procedure used in this research was reasonable and the amounts of

intermediates slightly above the resolution limit were true representatives of the transformation reactions.

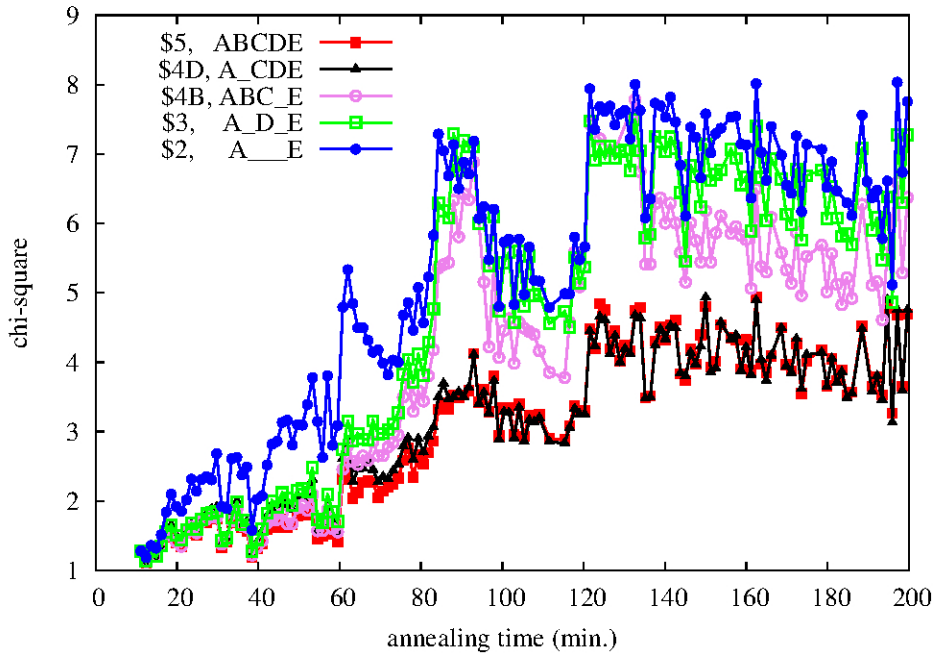

Fig. S3. The chi-square parameter for two, three four and five-component models for the full time span of the measurement.

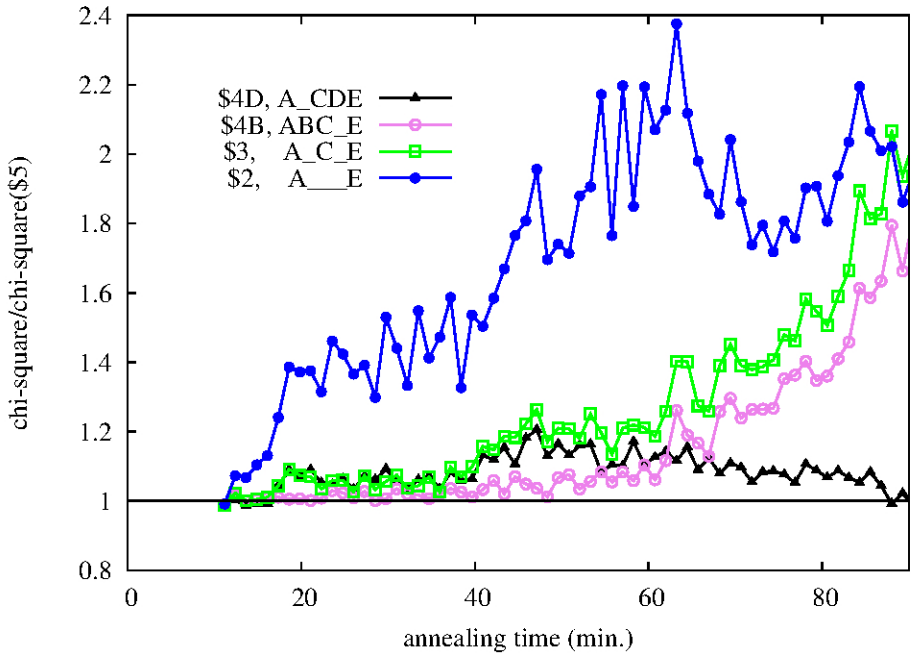

Fig. S4. The chi-square for different fitting models normalized to the 5-component model.

Tab. S1. Maximum relative amounts and hyperfine parameters of spectral components as derived from the NFS time spectra.

Component	Iron oxidation state	Max amount (%)	*IS* * (mm/s)	*Q* (mm/s)	*B* (T)
A	Fe(VI)	98 ± 1	–0.90 (fixed)	0	0
E	Fe(III)	90 ± 1	(0.10-0.15) ± 0.02	0.09 ± 0.01	(45.0-45.3) ± 0.3
C	Fe(III)	9 ± 2	0.30 ± 0.03	0.15 ± 0.05	(43.8-44.8) ± 0.5
D	Fe(IV)	5 ± 1	–0.30 ± 0.03	0.37 ± 0.03	0
B	Fe(V)	4 ± 1	–0.55 ± 0.04	0.15 ± 0.02	0

IS…isomer shift related to α-Fe at room temperature; Q…quadrupole splitting/shift; B…hyperfine magnetic field;
* Isomer shift values are related to room temperature, so they are not affected by the second order Doppler shift

Tab. S2. Proposed transformations from Fe(VI) to Fe(III) via Fe(V) and Fe(IV) in the thermal decomposition process at 235 °C.

Transformations	Time span (min)
$K_2Fe^{VI}O_4 \rightarrow KFe^{III}O_2 + 1/3(K_2O + KO_2) + 1/2\ O_2$	0 – 110
$2K_2Fe^{VI}O_4 \rightarrow KFe^{V}O_3 + K_3Fe^{III}O_3 + O_2$	0 – 110
$KFe^{V}O_3 \rightarrow KFe^{III}O_2 + 1/2\ O_2$	50 – 100*
$K_3Fe^{III}O_3 \rightarrow KFe^{III}O_2 + K_2O$	80 – 110**
$K_2Fe^{VI}O_4 \rightarrow K_2Fe^{IV}O_3 + 1/2\ O_2$	0 – 110
$K_2Fe^{IV}O_3 \rightarrow KFe^{III}O_2 + 1/3(K_2O + KO_2)$ ***	110 – 200
$K_2Fe^{VI}O_4 \rightarrow K_3Fe^{III}O_3 + KFe^{III}O_2 + 3/2\ O_2$	0 – 110
$K_3Fe^{III}O_3 \rightarrow KFe^{III}O_2 + K_2O$	80 – 110

* the beginning corresponds to the change of trend of (E) at 50 min

** the beginning corresponds to the change of trend of (E) at 80 min

*** this process is very slow (observable after 110 min)

References

(1) G. W. Thompson, G. W. Ockerman and J. M. Schreyer, *J. Am. Chem. Soc.,* 1951, **73**, 1379.

(2) H.-C. Wille, H. Franz, R. Röhlsberger, W. A. Caliebe and F.-U. Dill, *J. Phys.: Conf. Ser.*, 2010, **217**, 012008.

(3) J. B. Hastings, D. P. Siddons, U. Vanburck, R. Hollatz, U. Bergmann, *Phys. Rev. Let.,* 1991, **66(6)**, 770.

(4) Time spectrum: In fact, during a NFS experiment a time dependent intensity of the de-excited radiation, i.e. an interferogram, is detected. It consists of photons that are emitted by the system during its transition from the excited state into a ground state which occurs immediately after the synchrotron excitation pulse. Note that to get rid of the influence of the original excitation photons, the data acquisition starts with some time delay which is typically ~20 ns. Depending upon the number of nuclear energy levels governed by hyperfine interactions, usually photons of several energies (frequencies) sum up and construct a time-dependent signal. For the sake of simplicity, we will refer to these experimentally recorded data as 'time spectra'; though, strictly speaking, they are only a representation of nuclear level transitions in time domain.

(5) W. Sturhahn, E. Gerdau, *Phys. Rev. B,* 1994, **49**, 9285.